Location-based Spectrum Allocation and Partitioning Scheme for Cross-tier Interference Mitigation in Macro-Femtocell Networks

Sunheui Ryoo[a], Changhee Joo[b], Saewoong Bahk[a]

[a]*School of Electrical Engineering and Computer Science, INMC, Seoul National University, Seoul, Korea (e-mail: shryoo and sbahk@netlab.snu.ac.kr).*
[b]*School of Electrical and Computer Engineering, UNIST, Ulsan, Korea (e-mail: cjoo@unist.ac.kr).*

Abstract

In this paper, we solve the cross-tier interference problem in a two-tier network which consists of overlaid femtocells within a macrocell range. In the considered network, macro and femto base stations are assumed with the capabilities of power control and beamforming, differently from user terminals. Under such environments, we devise a decentralized solution where each femtocell determines whether to use shared spectrum or partitioned spectrum, considering users' location information, rather than using their detailed channel information. We derive distance thresholds beyond which the cross-tier interference is tolerable, and find an optimal shared spectrum ratio to maximize the network utility. Simulation results demonstrate that our decentralized scheme achieves comparable performance to the centralized one with low overhead and feedback delay.

Keywords: Femtocell, cross-tier interference mitigation, beamforming, spectrum allocation, location-based, decentralized algorithm.

1. Introduction

Femtocells have received great attention as a cost-effective high-bandwidth solution for next-generation wireless services. Femtocell networks can enhance indoor coverage by providing low power short range access points towards a wired infrastructure network. They operate in the licensed spectrum owned by a mobile operator and currently provides mobile convergence services in 3GPP LTE networks [1]. It has been shown that the femtocell approach is beneficial to both the service provider and users in many aspects such as network capacity, cell coverage, and battery consumption at user handsets [2].

The coexistence of macrocell and femtocell networks at a same spectrum, however, incurs additional control challenges due to the cross-tier interference between macrocell and femtocells as well as the co-tier interference. Although the co-tier interference control has been extensively studied in the literature [3, 4, 5, 6, 7, 8], the cross-tier interference control still has been an open problem and remains as a key technical challenge [2, 9].

Studies on the two-tier network have often assumed operator planned deployment of the microcell network where the cross-tier interference is somewhat tractable. They mainly have focused on uplink capacity in an overlaid macro and microcell network under code division multiple access (CDMA) environments [10, 11]. However, these approaches suffer from high deployment cost and low spatial spectrum reuse. To overcome these weaknesses, a low power user deployed femtocell network architecture has emerged as an attractive alternative [9]. Since femtocell networks are commonly deployed by subscribers, femto base stations (HeNBs) can be arbitrarily placed, which

makes the cross-tier interference problem more challenging.

When macro and femtocell networks coexist, it is desirable for the femtocells to generate minimal impact on the performance of the macrocell networks [1, 12]. To do so, an intuitive approach is assigning non-overlapped spectrums to the macrocell and femtocells, respectively [13]. However, this separate spectrum allocation limits spectrum bandwidth and accordingly degrades spectrum efficiency. The spectrum efficiency can be significantly improved by the cochannel deployment where macrocell and femtocells use the same spectrum [14].

With the goal of improving performance of both macrocell and femtocell users under the cochannel deployment, an MIMO beam subset selection strategy at microcells has been proposed in [15]. It maximizes the macrocell throughput by optimizing the trade-off relationship between multiplexing gain and multiuser interference, and also suppresses the cross-tier interference with a reduced number of beams. In [16], the authors have solved beamforming optimization problems that deal with total transmit power minimization, mean-square error balancing, and interference minimization. A centralized beamforming strategy that adaptively changes beam patterns and controls the transmit power at each cell is proposed in [17]. However, these cochannel deployments are still exposed to the cross-tier interference problem.

In [18], the authors have developed a way of hybrid spectrum use. This approach groups femtocells according to a distance threshold from the macro base station (MeNB) first. Differently from the macrocell, a group of femtocells use a partitioned spectrum, and the other group use the same spectrum with the macrocell. In [19], the cochannel operation is allowed for the fem-

tocells that are distant from the MeNB. To classify such cochannel HeNBs, the interference-limited coverage area has been estimated. However, these solutions are limited to the case of static network settings, and operate in a centralized manner that incurs significant cross-tier feedback delay. Therefore they are not suited for dynamic network environments where users actively join and leave the network. To reflect such dynamics, the frequency spectrum should be allocated in a short time without using detailed channel information.

In this paper, we develop a dynamic spectrum allocation and partitioning scheme according to users' location information to mitigate the cross-tier interference. Considering the beamforming gain, we design a novel decentralized scheme that partitions spectrum and decides which HeNBs to use the shared spectrum without requiring users' detailed channel information. The main contributions of this paper are three fold.

- We analytically obtain the average gain of beamforming transmission in a macro-femtocell network and formulate spectrum partitioning as a network utility maximization problem.

- We develop a low-complexity location-based solution to the spectrum allocation problem that requires minimal cross-tier feedback information. Then we find an optimal spectrum partitioning ratio to maximize the total cell utility.

- We confirm that our proposed scheme shows comparable performance to the centralized scheme that is impractical due to long cross-tier feedback delay.

The rest of this paper is organized as follows. In Section 2, we describe the system model and formulate the problem of spectrum allocation and partitioning as a network utility maximization problem. In Section 3, we consider a centralized spectrum allocation and partitioning scheme as a reference scheme. It finds a best set of shared femtocells but it is impractical due to cross-tier feedback delay. Then we develop a decentralized location-based scheme that uses distance thresholds, and find an optimal shared spectrum ratio to maximize the cell utility. In Section 4, we evaluate our decentralized location-based schemes through extensive simulations, and conclude our paper in Section 5.

2. System Model

We consider a two-tier network that consists of one macrocell and multiple femtocells. The MeNB is located at the center of the macrocell area with radius R_m. We assume that one mobile user denoted by MUE is randomly located, and connected to MeNB within the macrocell area. The femtocell networks are overlaid with the macrocell network, and provide closed access service to indoor subscribers. Each femtocell is randomly located within the macrocell area with density λ_f, and has an HeNB that covers the area of radius R_f ($R_f < R_m$). Let $\mathbf{K_t}$ denote the index set of all the HeNBs. Each HeNB$_i$ serves one femto user (HUE$_i$) at a time, which is randomly located within the associated femtocell area. In this paper, we focus on cross-tier interference between the macrocell and the femtocells. We do not consider co-tier interference, which has been extensively studied in the literature (e.g., see [3, 4, 5, 6, 7, 8]), and there are many solutions including conventional

multiple access techniques such as TDMA, SDMA, OFDMA, etc. In Fig. 2, for modeling we place the MeNB at the origin and denote the location vectors of HeNB_i, HUE_i, and MUE at time t by X_i, $Y_i(t)$, and $Z(t)$, respectively[1].

To mitigate cross-tier interference, we partition the available spectrum into two parts and then operate each part differently. The partitioning ratio can be decided dynamically according to given network environments. While the concept of the spectrum partitioning technique to mitigate interference has appeared in [18], [19], these approaches are limited to static spectrum partitioning. For ν portion of the spectrum, the macrocell has priority, and only non-interfering HeNBs can transmit simultaneously. For the rest $(1-\nu)$ portion, the macrocell is not allowed to transmit[2]. We express portion ν as *shared spectrum* and the other $(1-\nu)$ as *partitioned spectrum*.

Besides the spectrum partitioning, we utilize power control and beamforming transmission. We assume that base stations (MeNB and HeNBs) have capabilities of power control and beamforming transmission, while user devices (MUE and HUEs) do not due to the complexity and cost. In this paper, we study the performance of different beamforming configurations under the same transmission power setting regardless of the beamforming gain. To do so, we set the transmission power of MeNB to P_m^T such that the received signal strength at MUE equals P_m^R, assuming omnidirectional transmission

[1]Since most mobile devices (e.g., smart phone and smart pad) have the GPS function to support location-based services, we assume that the location information of the base stations and the users is available.

[2]Implicitly, we assume that there always exists a femtocell that generates cross-tier interference to the macrocell.

and no cross-tier interference. Similarly, we set the transmission power of HeNB_i to $P_{f_i}^T$ such that the received signal strength at HUE_i is P_f^R. MeNB and HeNBs use different transmission powers according to transmission link qualities to meet the required received signal strength.

Fig. 1 depicts an example of beamforming transmission for modeling [20]. Given the transmission power, there are two types of areas according to the antenna gain: main lobe and side lobe. Let θ denote the antenna (or beamforming) alignment angle between the transmitter and its target receiver, and θ_m denote the width of the main lobe in angle. The side lobe covers the remaining angle $(2\pi - \theta_m)$. The base station is configured with $N_b \in \{1, 4, 8\}$ beams, i.e. $\theta_m = \frac{2\pi}{N_b}$. Let g_m and g_s $(g_m > 1 > g_s)$ denote the antenna gains of the main lobe and the side lobe, respectively. If the receiver is located under the main lobe, i.e. $\theta \leq \theta_m$, the received signal will be strengthened by g_m, and otherwise, weakened by g_s. Hence, the received signal strength depends on the antenna alignment angle θ. In this paper, we assume *perfect antenna control*, where MeNB and HeNBs perfectly control transmission power and directs its beam toward the target receiver to achieve the main lobe gain of g_m.

We derive the average SIR gain of beamforming transmission over omnidirectional transmission. Considering the transmission power control, we have

$$\begin{aligned} P_m^T(t) &= \frac{P_m^R |Z(t)|^\alpha}{g_m}, \\ P_{f_i}^T(t) &= \frac{P_f^R |X_i - Y_i(t)|^\alpha}{g_m}, \end{aligned} \tag{1}$$

where α denotes the path loss exponent. Afterwards we omit variable t if there is no confusion. Let $y_i I_i^h$ denote the cross-tier interference from MeNB to HUE_i, and $x_i I_i^m$ denote the cross-tier interference from HeNB_i to MUE, where y_i represents the beamforming gain indicator with $y_i = g_m$, if HUE_i is located within the main lobe of MeNB, and $y_i = g_s$, otherwise. Similarly, x_i represents the beamforming gain according to the location of MUE with respect to HeNB_i. Then we have

$$\begin{aligned} y_i I_i^h &= \frac{y_i P_m^T}{|Y_i|^\alpha} = \frac{y_i P_m^R |Z|^\alpha}{g_m |Y_i|^\alpha}, \\ x_i I_i^m &= \frac{x_i P_{f_i}^T}{|X_i - Z|^\alpha} = \frac{x_i P_f^R |X_i - Y_i|^\alpha}{g_m |X_i - Z|^\alpha}. \end{aligned} \tag{2}$$

We assume that the data transmission is successful if the received signal strength is not smaller than a certain threshold. Let γ_m^{th} and γ_f^{th} denote the required SIR thresholds[3] for MUE and HUE, respectively. Also, let γ_m and γ_{f_i} denote the received SIRs at MUE and HUE_i, respectively, and $\mathbf{K_s}$ denote the index set of HeNBs that can have successful transmission with the shared spectrum. Each communication of HeNB_i for $i \in \mathbf{K_s}$ is successful if

$$\gamma_{f_i} = \frac{P_f^R}{y_i I_i^h} \geq \gamma_f^{th}, \tag{3}$$

and the macrocell communication is successful if

$$\gamma_m = \frac{P_m^R}{\sum_{i \in \mathbf{K_s}} x_i I_i^m} \geq \gamma_m^{th}. \tag{4}$$

Let $\mathbf{K_p}$ denote the index set of active HeNB_i that use only the partitioned spectrum. Each HeNB_i in $\mathbf{K_p}$ is assumed to transmit successfully owing

[3]These can be interpreted as QoS parameter values that are required by subscribers.

to the power control and no cross-tier interference. Then the average SIR gain at MUE and HUE of beamforming transmission with N_b beams over omnidirectional transmission is

$$\Psi(N_b) = \frac{g_m N_b}{(N_b - 1)\, g_s + g_m}. \tag{5}$$

For a successful transmission that satisfies equations (3) and (4), we consider that the link achieves the Shannon capacity. When we normalize each link capacity by the entire spectrum bandwidth, each downlink of MeNB, HeNB$_i$ for $i \in \mathbf{K_s}$, and HeNB$_j$ for $j \in \mathbf{K_p}$ achieves $C_m := \nu \log(1 + \gamma_m)$, $C_{f_i} := \log(1 + \gamma_{f_i})$, and $C_{f_j} := (1 - \nu) \log(1 + \gamma_{f_j})$, respectively. We define user's utility as a logarithmic function of the achieved link rate [21], then the total utility U is

$$U = w_m \log C_m + w_f \sum_{i \in \mathbf{K_s}} \log C_{f_i} + w_f \sum_{j \in \mathbf{K_p}} \log C_{f_j}, \tag{6}$$

where w_m and w_f are relative weights for macrocell and femtocell utilities, respectively. In this paper, we maximize the total utility by suppressing the cross-tier interference,

$$\underset{\nu, \mathbf{K_s}, \mathbf{K_p}}{\text{maximize}} \quad U. \tag{7}$$

We allocate the partitioned spectrum to femtocells that are severely interfering with MUE or MeNB, and estimate the optimal ratio of shared spectrum in Section 3.

3. Location-based Spectrum Allocation and Partitioning

Our network utility maximization problem (7) can be decomposed into two subproblems of spectrum allocation and partitioning. The former determines which HeNBs are to be allocated to the partitioned spectrum, and the latter handles how much spectrum should be reserved for the partitioned spectrum. In this section, we develop a centralized spectrum allocation and partitioning scheme, and then propose a decentralized solution by using users' location information.

We start with a centralized spectrum allocation (CSA) scheme with greedy approximation as a reference scheme. Suppose that a central controller has all the channel information about MeNB, MUE, HeNBs, and HUEs.The controller collects all the information, finds an optimal solution, and distributes the results to MeNB, MUE, HeNBs, and HUEs. The detailed procedures are given as follows.

1. To check the cross-tier interference from MeNB to HUEs (3), MeNB transmits the pilot signal and each HUE measures the received pilot signal strength. The decision results of each HUE is delivered to the central controller through the backhaul network.
2. To check the cross-tier interference from HeNBs to MUE (4), the controller should know the level of cross-tier interference from each HeNB that satisfies equation (3). Once all the information is collected, the controller finds an optimal subset of HeNBs by solving equation (7) directly. This procedure requires high computational complexity.
3. To reduce the complexity, a greedy approximation is used, where the central controller sorts HeNBs in the increasing order of the interference

level. Starting from an empty set, it sequentially adds an HeNB to this set in order and stops adding if equation (4) is not valid. The resultant set contains a largest number of HeNBs that satisfy equation (4). The controller allocates the full spectrum to the HeNBs in this set (i.e. $\mathbf{K_s}$) and the partitioned spectrum to the rest.

4. The central controller determines the shared spectrum ratio, which will be given in Section 3.2. Then it distributes the decision results to MeNB, MUE, HeNBs and HUEs.

Although the above centralized approach lowers the complexity owing to the greedy approximation, it is still infeasible in practice, particularly when there are many HeNBs and HUEs in the network. Another problem is that since the central controller collects all the channel information from HeNBs through the backhaul network, it incurs long cross-tier feedback delay and can be hardly accomplished within a short channel coherence time [2].

Due to the high message overhead and cross-tier feedback delay in the centralized solution, we are motivated to devise a simple decentralized solution that does not require detailed channel information. Because a receiver experiences much lower interference as it is getting away from the interferer, a femtocell network that is to a certain extent away from MeNB and MUE, is enabled to use the same spectrum with the macrocell network. We introduce two distance thresholds: femto distance threshold d_f^{th} and macro distance threshold d_m^{th}. The femto distance threshold, d_f^{th} represents the distance from MeNB, beyond which MeNB incurs negligible cross-interference to HUE. Similarly the macro distance threshold d_m^{th}, represents the distance from MUE, beyond which HeNB incurs negligible cross-tier interference to

MUE. Using these two thresholds, we describe a decentralized location-based spectrum allocation (LSA) scheme as follows (see Algorithm 1 also).

1. MeNB determines two distance thresholds d_m^{th}, d_f^{th}, and the shared spectrum ratio ν, and inform HeNBs of these through the backhaul network.
2. Each HUE_i examines whether its effective distance from MeNB is greater than d_f^{th} or not. This accounts for the effectiveness of the beamforming gain, and checks the cross-interference from MeNB to HUE_i (line 4 in Algorithm 1).
3. Each HeNB_i examines whether its distance from MUE is greater than d_m^{th}. This checks the cross-tier interference from HeNB_i to MUE (line 4 in Algorithm 1).
4. If HeNB_i passes the above two tests, it belongs to $\mathbf{K_s}$ and uses the full spectrum. Otherwise, it belongs to $\mathbf{K_p}$ and uses the partitioned spectrum.

Because the proposed decentralized LSA scheme does not require any channel information, it does not incur cross-tier channel feedback delay. Fig. 3 compares the message exchanges between the base stations and MUE, HUE in CSA and LSA schemes. In the following subsections, we analytically obtain the two distance thresholds d_f^{th}, d_m^{th} and the shared spectrum ratio ν.

3.1. Spectrum allocation

In this subsection, we analytically find two distance thresholds, d_f^{th} and d_m^{th}. HeNBs are permitted to use the same spectrum with the macrocell network, only when they satisfy the SIR requirements (3) and (4). Thus, we transform these two received SIR requirements into two distance thresholds,

assuming that the femtocell networks and the associated users are randomly distributed[4].

We start to calculate d_f^{th} considering the cross-tier interference from MeNB to HUE_i. For a femtocell to share the spectrum with the macrocell, it is required that the received SIR at HUE_i is no smaller than the SIR requirement, i.e. $\gamma_{f_i} \geq \gamma_f^{th}$. We define d_f^{th} as the distance from MeNB such that the SIR at an HUE is equal to γ_f^{th} under omnidirectional transmission, i.e.

$$d_f^{th} := \min \left\{ |Y_i| \; \middle| \; \frac{P_f^R}{I_i^h} \geq \gamma_f^{th} \right\}.$$

Combining this with equations (2) and (3), we have $\frac{P_f^R g_m (d_f^{th})^\alpha}{P_m^R |Z|^\alpha} = \gamma_f^{th}$. Hence, we obtain

$$d_f^{th} = \left(\frac{\gamma_f^{th} P_m^R}{g_m P_f^R} \right)^{\frac{1}{\alpha}} |Z|. \tag{8}$$

As the SIR requirement γ_f^{th} gets smaller and the distance $|Z|$ between MeNB and MUE decreases, the threshold d_f^{th} gets smaller. This implies that more HeNBs are allowed to use the full spectrum. This is because an HUE is more tolerant to the interference with γ_f^{th} smaller, or the interference from MeNB decreases as the transmission power of MeNB and $|Z|$ decrease. Considering the beam gain y_i, we denote the index set of HeNB_i that satisfy $|Y_i| \geq y_i^{\frac{1}{\alpha}} d_f^{th}$ by $\mathbf{F_s}$, and the other HeNBs with $|Y_i| < y_i^{\frac{1}{\alpha}} d_f^{th}$ by $\mathbf{F_p}$.

Similarly, we can calculate d_m^{th} with the cross-tier interference from HeNBs

[4]In general, location information is not the only factor that expresses cross-tier interference and channel condition. Therefore in our simulations, we verify LSA scheme under both uniformly distributed and densely deployed hotspot topologies, assuming that each user experiences a different path loss exponent in Section 4.

to MUE, which is defined as the distance such that the SIR of MUE equals γ_m^{th},

$$d_m^{th} := \min\left\{ d \;\middle|\; \frac{P_m^R}{\mathrm{E}[\sum_{i\in\mathbf{F_s}\cap\{|X_i-Z|\geq d\}} x_i I_i^m]} \geq \gamma_m^{th} \right\}.$$

For d_f^{th}, we need to consider only one interferer MeNB, but for d_m^{th}, multiple interferers of HeNBs. Let $\mathbf{M_s}$ denote the index set of HeNBs whose distance from MUE is not smaller than d_m^{th}, i.e. $\mathbf{M_s} := \{i \mid |X_i - Z| \geq d_m^{th}\}$, and $\mathbf{M_p}$ denote the rest, i.e. $\mathbf{M_p} := \mathbf{K_t}\backslash\mathbf{M_s}$. And we have $\mathbf{K_s} = \mathbf{F_s} \cap \mathbf{M_s}$.

From $\mathbf{K_s} \subset \mathbf{M_s}$ and independent locations of HeNBs, we have the average cross-tier interference at MUE as

$$\begin{aligned} \mathrm{E}\left[\sum_{i\in\mathbf{K_s}} x_i I_i^m\right] &\leq \mathrm{E}\left[\sum_{i\in\mathbf{M_s}} x_i I_i^m\right] \\ &= \mathrm{E}\left[x_i I_i^m | \mathbf{M_s}\right] \cdot \mathrm{E}[|\mathbf{M_s}|] \leq \frac{P_m^R}{\gamma_m^{th}}, \end{aligned} \tag{9}$$

where the last inequality constraint comes from the interference requirement (4).

From (2) and the independence assumption between X_i, Y_i, and Z, we have

$$\begin{aligned} \mathrm{E}\left[x_i I_i^m | \mathbf{M_s}\right] &= \mathrm{E}\left[\frac{x_i P_f^R}{g_m} \frac{|X_i - Y_i|^\alpha}{|X_i - Z|^\alpha} \;\middle|\; \mathbf{M_s}\right] \\ &= P_f^R \cdot \mathrm{E}\left[\frac{x_i}{g_m}\right] \cdot \mathrm{E}\left[|X_i - Y_i|^\alpha\right] \cdot \mathrm{E}\left[|X_i - Z|^{-\alpha} | \mathbf{M_s}\right] \\ &\geq \frac{P_f^R}{\Psi(N_b)} \cdot \int_0^{R_f} p^\alpha \frac{2p}{R_f^2} dp \cdot \int_{d_m^{th}}^{R_m} q^{-\alpha} \frac{2q}{R_m^2} dq \\ &= \frac{4 P_f^R R_f^{\alpha+2}}{\Psi(N_b) R_m^2 R_f^2 (\alpha^2 - 4)} \left({d_m^{th}}^{-\alpha+2} - {R_m}^{-\alpha+2} \right), \end{aligned} \tag{10}$$

where $\Psi(N_b)$ denotes the average beamforming gain with N_b configuration

over the omnidirectional transmission, and satisfies $\Psi(N_b) = \mathrm{E}\left[\frac{g_m}{x_i}\right] \geq \frac{g_m}{\mathrm{E}[x_i]}$ by Jensen's inequality.

Also we obtain $\mathrm{E}[|\mathbf{M_s}|]$ as

$$\mathrm{E}[|\mathbf{M_s}|] = \int_0^{2\pi} \int_{d_m^{th}}^{R_m} \lambda_f \cdot r \; dr d\theta = \frac{|\mathbf{K_t}|}{R_m^2} \left(R_m^2 - {d_m^{th}}^2 \right), \tag{11}$$

since the HeNB density is given as $\lambda_f = \frac{|\mathbf{K_t}|}{\pi R_m^2}$.

Substituting equations (10) and (11) into (9), we obtain the upper bound of d_m^{th} by solving the following equation.

$$(R_m)^{-\alpha+2} \left(d_m^{th}\right)^2 - \left(d_m^{th}\right)^{-\alpha+4} + R_m^2 \left(d_m^{th}\right)^{-\alpha+2} = \frac{\Psi(N_b) R_m^4 P_m^R \left(\alpha^2 - 4\right)}{4\gamma_m^{th} P_f^R R_f^{\alpha} |\mathbf{K_t}|} + (R_m)^{-\alpha+4},$$

where the solution can be numerically obtained. For the path loss exponent of $\alpha = 4$, we can obtain the closed form solution as

$$d_m^{th}|_{\alpha=4} \leq R_m \sqrt{\frac{f(\cdot) - \sqrt{f(\cdot)^2 - 4}}{2}}. \tag{12}$$

where $f(|\mathbf{K_t}|, \Psi(N_b), \gamma_m^{th}) := \frac{3\Psi(N_b) P_m^R}{\gamma_m^{th} P_f^R |\mathbf{K_t}|} \left(\frac{R_m}{R_f}\right)^4 + 2$, which increases (and d_m^{th} decreases) with the number of beams N_b, and decreases (and d_m^{th} increases) with higher γ_m^{th} and larger $|\mathbf{K_t}|$.

3.2. Spectrum partitioning

In this subsection, we analytically derive the shared spectrum ratio ν to maximize the total utility using two distance thresholds. So we rewrite the total cell utility (6) as

$$\begin{aligned} U = {} & w_m \log \nu + w_f |\mathbf{K_p}| \log(1-\nu) + w_m \log(\log(1+\gamma_m)) \\ & + w_f \log \left(\prod_{i \in \mathbf{K_s}} \log(1+\gamma_{f_i}) \right) + w_f \log \left(\prod_{j \in \mathbf{K_p}} \log(1+\gamma_{f_j}) \right). \end{aligned} \tag{13}$$

For any given $\mathbf{K_p}$, $\mathbf{K_s}$, $\{\gamma_{f_i}\}$, and $\{\gamma_{f_j}\}$, the function is concave with respect to ν. Then we obtain the optimal shared spectrum ratio ν^* as

$$\nu^* = \frac{w_m}{w_f|\mathbf{K_p}| + w_m}. \tag{14}$$

Recall that $|\mathbf{K_p}|$ denotes the number of femtocells that use the partitioned spectrum and $\mathbf{K_p} = \mathbf{F_p} \cup \mathbf{M_p}$. Since obtaining an exact number $|\mathbf{K_p}|$ requires feedback information from all the HeNBs, which incurs cross-tier feedback delay, we use $|\mathbf{F_p}| + |\mathbf{M_p}|$ ($\geq |\mathbf{K_p}|$) and their expectations.

We first calculate the expectation $\mathrm{E}[|\mathbf{F_p}|]$. Assuming that UEs (i.e. MUE and HUEs) and HeNBs are randomly distributed, the probability that HUE_i is located under the main lobe of MeNB is $\frac{1}{N_b}$. Thus we can calculate the average antenna gain $E[y_i]$ as $\mathrm{E}[y_i] = \frac{1}{N_b} g_m + \frac{N_b - 1}{N_b} g_s$. Since HeNB_i belongs to $\mathbf{F_p}$ when $|Y_i| \geq y_i^{\frac{1}{\alpha}} d_f^{th}$, we can calculate $\mathrm{E}[|\mathbf{F_p}|]$ by taking the expectation as

$$\begin{aligned}
\mathrm{E}[|\mathbf{F_p}|] &= \lambda_f \cdot \pi \mathrm{E}\left[\left(y_i^{\frac{1}{\alpha}} d_f^{th}\right)^2\right] \\
&= \frac{|\mathbf{K_t}|}{R_m^2} \cdot \mathrm{E}\left[\left(y_i^{\frac{1}{\alpha}} \left(\frac{\gamma_f^{th} P_m^R}{g_m P_f^R}\right)^{\frac{1}{\alpha}} |Z|\right)^2\right] \\
&\leq \frac{|\mathbf{K_t}| \cdot \mathrm{E}[|Z|^2]}{R_m^2} \left(\frac{\gamma_f^{th} P_m^R}{g_m P_f^R} \cdot \mathrm{E}[y_i]\right)^{\frac{2}{\alpha}} \\
&= \frac{|\mathbf{K_t}| \cdot \mathrm{E}[|Z|^2]}{R_m^2} \left(\frac{\gamma_f^{th} P_m^R}{P_f^R N_b} \left(1 + \frac{g_s(N_b - 1)}{g_m}\right)\right)^{\frac{2}{\alpha}},
\end{aligned} \tag{15}$$

where the inequality holds according to Jensen's inequality when $\alpha \geq 2$. Then we denote the right side of (15) by $\widetilde{\mathrm{E}[|\mathbf{F_p}|]}$. Using the fact that

$\mathrm{E}[|\mathbf{M_p}|] = |\mathbf{K_t}| - \mathrm{E}[|\mathbf{M_s}|]$ and (11), we are able to partition the spectrum bandwidth according to the approximate value $\hat{\nu}$ defined as

$$\hat{\nu} := \frac{w_m}{w_f(\widetilde{\mathrm{E}[|\mathbf{F_p}|]} + \mathrm{E}[|\mathbf{M_p}|]) + w_m}. \tag{16}$$

Because $\mathrm{E}[|\mathbf{F_p}|] \leq \widetilde{\mathrm{E}[|\mathbf{F_p}|]}$, $\hat{\nu}$ is an underestimator that satisfies

$$\begin{aligned} \hat{\nu} &\leq \frac{w_m}{w_f(\mathrm{E}[|\mathbf{F_p}|] + \mathrm{E}[|\mathbf{M_p}|]) + w_m} \\ &\leq \frac{w_m}{w_f(\mathrm{E}[|\mathbf{K_p}|]) + w_m} \leq \mathrm{E}[\nu^*]. \end{aligned} \tag{17}$$

Therefore, this underestimation leads to some performance degradation, which will be investigated in the following section.

4. Performance Evaluation

In this section, we compare our LSA scheme with the other two competitive schemes in terms of cell utility and cell capacity. One is the CSA scheme, and the other is a scheme that does not use spectrum partitioning, denoted as no-spectrum-partitioning-and-allocation (NSA) scheme. In the NSA scheme, as the spectrum is not partitioned, and MeNB and HeNBs share the full spectrum, there exists severe cross-tier interference.

We consider 100 femtocells within a macrocell coverage, where MeNB is located at the center and has the transmission range of $R_m = 500$ m. Each HeNB is randomly located within the macrocell and has the transmission range of $R_f = 20$ m. MUE and HUEs are also randomly located within the transmission range of each associated base station. The utility weights for MUE and HUEs are set to $\omega_m = 20$ and $\omega_f = 1$, respectively. We simulate the

macro-femtocell network with the spectrum bandwidth of 20 MHz, varying the required SIR level and the number of beams $N_b \in \{1, 4, 8\}$.

For each case, we generate $10,000$ different random topologies and obtain their average performance. By changing the beamforming sharpness (i.e. $\theta_m = \frac{2\pi}{N_b}$), beam gains of main beam g_m and side beam g_s are shown in Table 1. The average beamforming gain $\Psi(N_b)$ in the macro-femtocell network is also calculated from (5). Although we assume an identical path loss parameter α in our analysis, it would be different in reality for each link due to different wireless channel environments such as multi-path fading and wall penetration. In our simulations, each link has a different α that is randomly chosen in $[3, 5]$. Such per link information is not given to the LSA scheme, and we configure LSA with the average α of 4. The other detailed parameter values for wireless communications follow the 3GPP LTE specifications [22], which are provided in Table 1.

Fig. 4 shows the cell utility and the cell capacity with different beam configurations when $\gamma^{th} = 8$ dB. As expected, the total cell utility increases with sharper beams owing to reduced cross-tier interference. In each beam configuration, LSA outperforms NSA and achieves comparable performance to CSA. With shaper beams, NSA shows significant performance improvement according to the reduced interference, while CSA and LSA achieve moderate improvements. This is because CSA and LSA are already successful in mitigating the cross-tier interference by using the spectrum allocation and partitioning scheme. In Fig. 4a, we observe that there is not much improvement in utility due to the concavity of the utility function. Fig. 4b shows the cell capacity for each scenario. The beamforming technology significantly

improves the cell capacity. CSA sometimes performs poorly compared to LSA in capacity because its objective is to maximize the utility which counts both capacity and fairness.

Fig. 5 shows the average number of HeNBs that share the spectrum with MeNB, i.e $E[|\mathbf{K_s}|]$. In general, a larger $|\mathbf{K_s}|$ leads to higher spectrum efficiency. In Fig. 5, LSA achieves as the same level of efficiency as CSA. The spectrum efficiency improves with the number of beams due to less cross-tier interference, and decreases with more stringent SIR requirements since a smaller number of HeNBs are allowed to share the full spectrum.

In Fig. 5we present the performance of LSA when femtocells are no longer uniformly distributed and there exists severe interference around MUE. In such a scenario, within the macrocell site, we consider a circular area of radius $\frac{1}{4}R_m$ centered at the MUE. Among $|\mathbf{K_t}|$ HeNBs, k_{in} HeNBs are randomly located inside the circular area, and the rest outside the circular area. We define the femtocell density bias δ_f as the ratio of k_{in} to $|\mathbf{K_t}|$. So the simulations for uniform distribution uses $\delta_f = 1/16$. As δ_f increases, HeNBs are more densely placed in the inner circular area around MUE.

Fig. 7 shows the cell utility and the cell capacity with different femtocell density biases when $N_b = 4$ and $\gamma^{th} = 8$ dB. As the femtocells are densely located within the small area, the cell utility and the cell capacity moderately decrease because of high cross-tier interference. It also shows that LSA still achieves the cell utility comparable to CSA, but the performance gap becomes larger. When HeNBs are crowded around MUE, the CSA scheme mitigates severe interference by allocating HeNBs around MUE to the partitioned spectrum with the perfect channel information. In contrast, LSA

still allocates the partitioned spectrum first to those HeNBs that are close to MeNB due to the lack of exact channel information. Nonetheless, LSA significantly outperforms NSA. Under a low femtocell density bias, LSA achieves a larger cell capacity than CSA. This is due to that the objective of our spectrum partitioning is to maximize the cell utility, rather than the cell capacity.

Overall, our simulations show that LSA achieves comparable performance to CSA. It is an interesting result that LSA can mitigate cross-tier interference successfully under dynamic network environments without using users' detailed channel information. By allowing only the HeNBs that are distant from MeNB and MUE to share the spectrum with the macrocell network, it successfully removes the necessity of detailed channel information at a slight loss in performance gain.

5. Conclusion

In this paper, we addressed the downlink cross-tier interference problem in a macro-femtocell networks with power control and beamforming transmission. To solve this problem, we developed a location-based spectrum allocation and partitioning scheme that requires no channel feedback information. Our solution classifies femtocells that generate high cross-tier interference, and allocate them the partitioned spectrum. Under the assumption that femtocells are uniformly distributed within the macrocell area, we analytically obtained distance thresholds beyond which the cross-tier interference is tolerable. Using these results, we obtained an optimal shared spectrum ratio to maximize the cell utility. Through extensive simulations, we showed that

our location-based scheme successfully approximates the centralized scheme that requires detailed channel feedback information and makes significant improvement over the conventional cochannel deployment of macro and femtocells.

References

[1] 3rd Generation Partnership Project (3GPP), Technical Specification Group Radio Access Network, 3GPP TR 25.820 (2008).

[2] V. Chandrasekhar, J. Andrews, A. Gatherer, Communications Magazine, IEEE 46 (2008) 59–67.

[3] B. Kim, J. Kwon, J. Lee, in: Computer Communications and Networks (ICCCN), 2011 Proceedings of 20th International Conference on, IEEE, pp. 1–6.

[4] D. López-Pérez, A. Valcarce, G. De La Roche, J. Zhang, Communications Magazine, IEEE 47 (2009) 41–48.

[5] C. Oh, M. Chung, H. Choo, T. Lee, Computational Science and Its Applications–ICCSA 2010 (2010) 96–106.

[6] K. Sundaresan, S. Rangarajan, in: Proceedings of the tenth ACM international symposium on Mobile ad hoc networking and computing, ACM, pp. 33–42.

[7] W. Park, S. Bahk, Computer Communications 32 (2009) 703–711.

[8] C. Chen, C. Wang, S. Chao, H. Wei, ACM SIGMOBILE Mobile Computing and Communications Review 14 (2010) 13–15.

[9] V. Chandrasekhar, J. Andrews, Wireless Communications, IEEE Transactions on 8 (2009) 3498–3509.

[10] S. Kishore, L. Greenstein, H. Poor, S. Schwartz, Wireless Communications, IEEE Transactions on 5 (2006) 1333–1342.

[11] C. Kang, H. Cho, D. Sung, Vehicular Technology, IEEE Transactions on 52 (2003) 333–346.

[12] Y. Kim, S. Lee, D. Hong, Wireless Communications, IEEE Transactions on 9 (2010) 2695–2700.

[13] V. Chandrasekhar, J. Andrews, Communications, IEEE Transactions on 57 (2009) 3059–3068.

[14] H. Claussen, in: Personal, Indoor and Mobile Radio Communications, IEEE 18th International Symposium on, IEEE, pp. 1–5.

[15] S. Park, W. Seo, Y. Kim, S. Lim, D. Hong, Wireless Communications, IEEE Transactions on 9 (2010) 3440–3449.

[16] Y. Jeong, T. Quek, H. Shin, Journal of Communication and Networks 13 (2011) 327–338.

[17] C. You, Y. Jung, S. Cho, Journal of Communication and Networks 13 (2011) 319–326.

[18] Y. Bai, J. Zhou, L. Chen, in: Proceedings of the 28th IEEE conference on Global telecommunications, IEEE, pp. 1642–1647.

[19] I. Guvenc, M. Jeong, F. Watanabe, H. Inamura, Communications Letters, IEEE 12 (2008) 880–882.

[20] R. Ramanathan, in: Proceedings of the 2nd ACM international symposium on Mobile ad hoc networking & computing, ACM, pp. 95–105.

[21] J. Choi, S. Bahk, Vehicular Technology, IEEE Transactions on 56 (2007) 766–778.

[22] Alcatel-Lucent, picoChip Designs, Vodafone, 3GPP Standard Contribution (R4-092042) (May 2009).

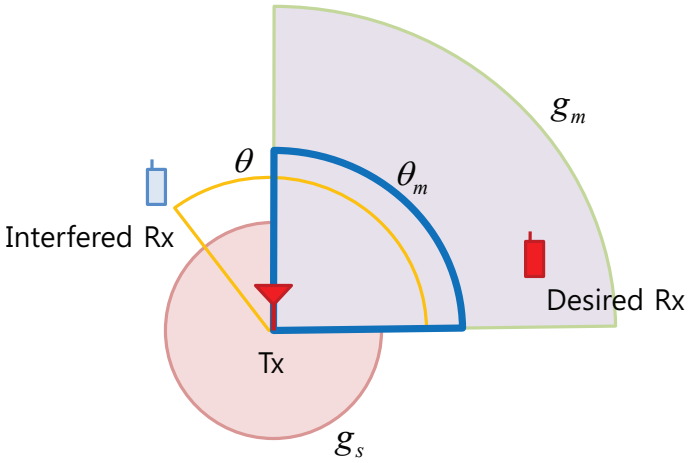

Figure 1: Beamforming transmission model.

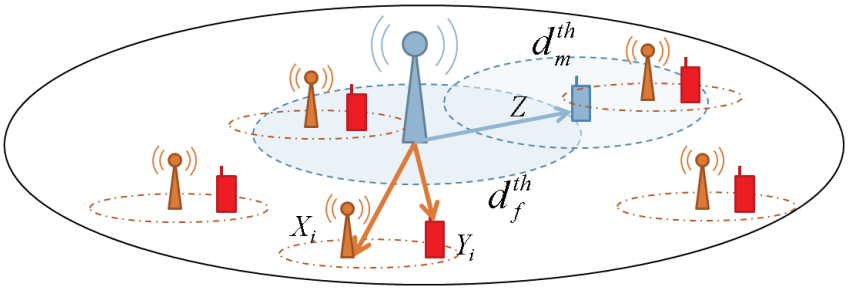

Figure 2: Deployment model, distance thresholds and location vectors of macro and femtocells.

Algorithm 1 Location-based Spectrum Allocation (LSA)

MeNB calculates d_f^{th}, d_m^{th} and ν, and informs HeNBs of d_f^{th}, d_m^{th}, ν, and Z through the backhaul network.
for each HeNB$_i$ **do**
    Find y_i with the locations of Z, Y_i.
    if $|Y_i| \geq y_i^{\frac{1}{\alpha}} d_f^{th}$ and $|X_i - Z| \geq d_m^{th}$ **then**
        HeNB$_i \in \mathbf{K_s}$
    else
        HeNB$_i \in \mathbf{K_p}$
    end if
end for
if HeNB$_i \in \mathbf{K_s}$ **then**
    HeNB$_i$ uses the full spectrum.
else
    HeNB$_i$ uses the partitioned spectrum.
end if

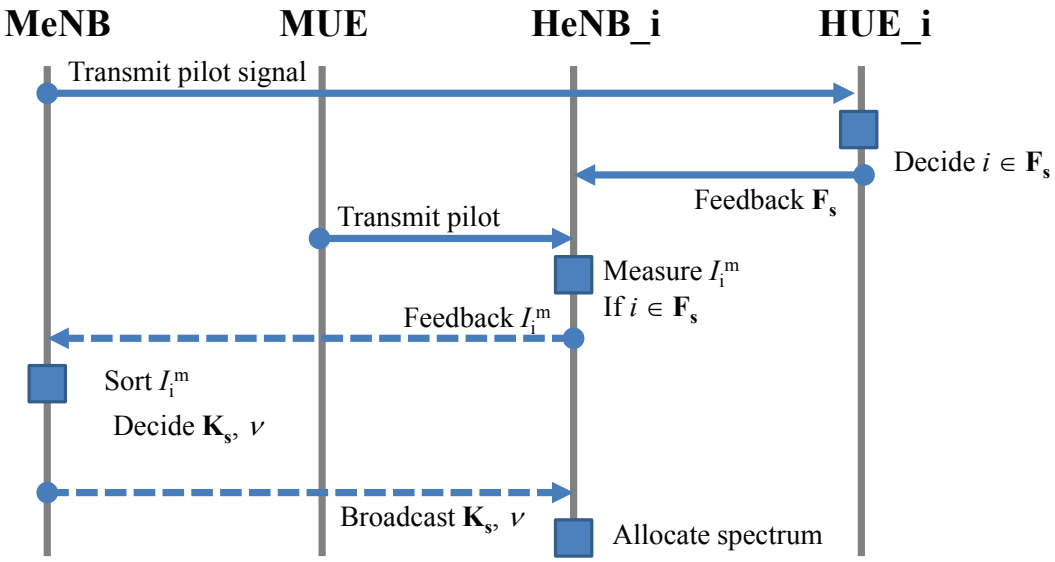

(a) CSA scheme

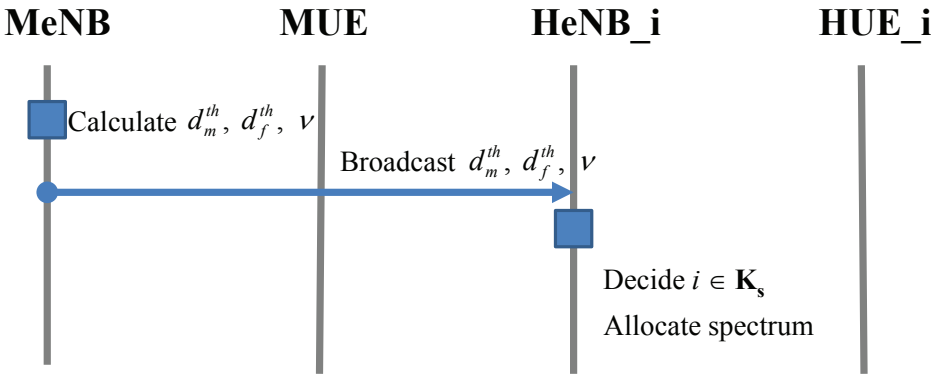

(b) LSA scheme

Figure 3: Message exchange diagram in CSA and LSA schemes.

Table 1: Simulation Parameters

<table>
<tr><td colspan="3">System Model</td></tr>
<tr><td rowspan="2">Macrocell</td><td>Transmission range</td><td>R_m = 500 m</td></tr>
<tr><td>Maximum power</td><td>46 dBm</td></tr>
<tr><td rowspan="2">Femtocell</td><td>Transmission range</td><td>R_f = 20 m</td></tr>
<tr><td>Maximum power</td><td>20 dBm</td></tr>
<tr><td rowspan="2">Beamforming</td><td>BSs</td><td><table><tr><th>N_b</th><th>g_m</th><th>g_s</th><th>$\Psi(N_b)$</th></tr><tr><td>1</td><td>0.0</td><td>0</td><td>0.0</td></tr><tr><td>4</td><td>9.8</td><td>-30</td><td>6.0</td></tr><tr><td>8</td><td>18.4</td><td>-30</td><td>9.0</td></tr></table></td></tr>
<tr><td>UEs</td><td>0 dB (N_b=1)</td></tr>
<tr><td colspan="3">Channel model</td></tr>
<tr><td colspan="2">UE noise figure</td><td>-174 dBm per Hz</td></tr>
<tr><td colspan="2">Spectrum bandwidth</td><td>20 MHz</td></tr>
</table>

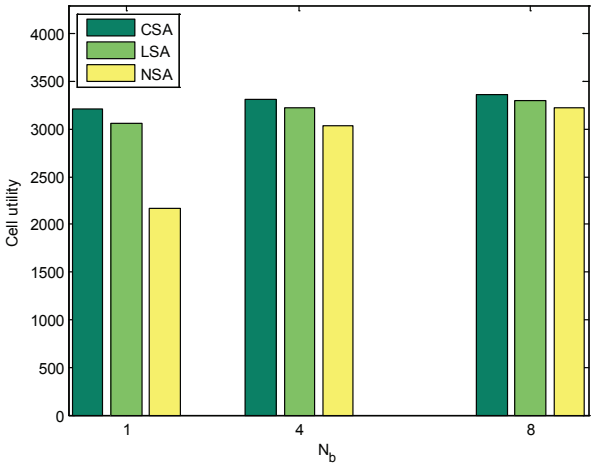

(a) Cell utility

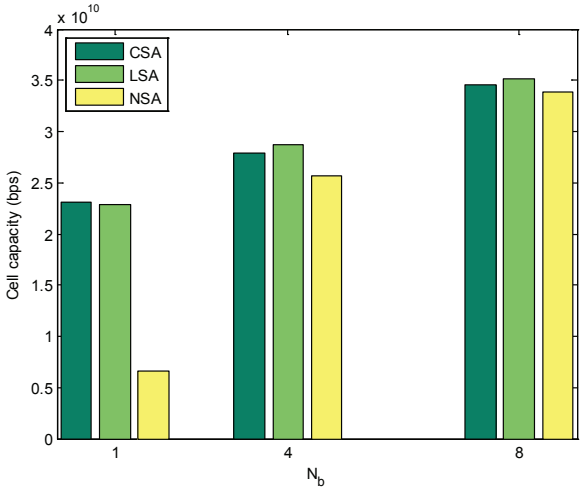

(b) Cell capacity

Figure 4: Performance of CSA, LSA, and NSA with different beam configurations when $\gamma^{th} = 8$ dB. The cell utility improves with the number of beams. CSA and LSA show less improvement since they successfully manage interference already through the spectrum partitioning. The improvement in cell capacity is more observable than that in utility due to the concavity of the utility function.

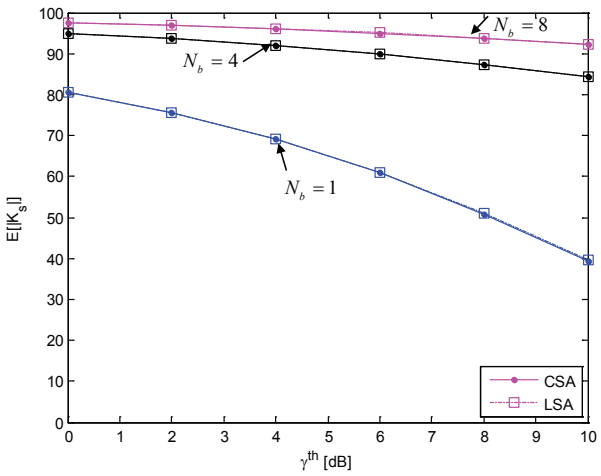

Figure 5: Average $|\mathbf{K_s}|$ with different required SIRs γ^{th}. To reduce the cross-tier interference to the macrocell, the number of HeNBs $|\mathbf{K_s}|$ that share the spectrum with the macrocell decreases as the SIR requirement becomes more stringent. On the other hand, it increases with larger N_b since higher beamforming gain makes the system more tolerable to the cross-tier interference.

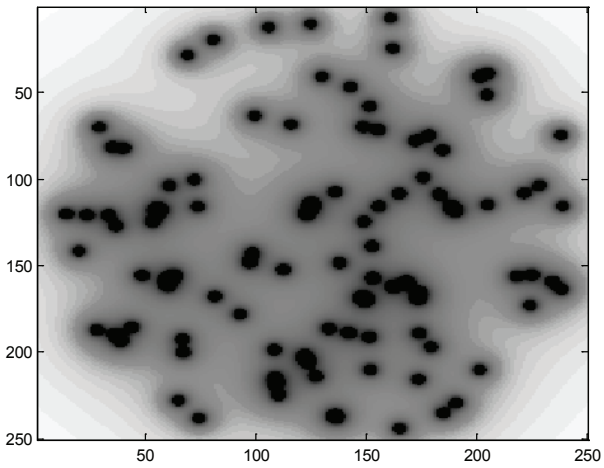

(a) Randomly distributed topology

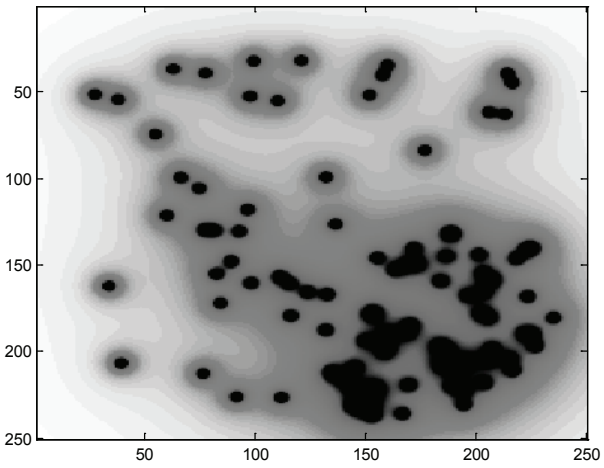

(b) Biased distributed topology

Figure 6: Example of randomly and biased distributed topology.

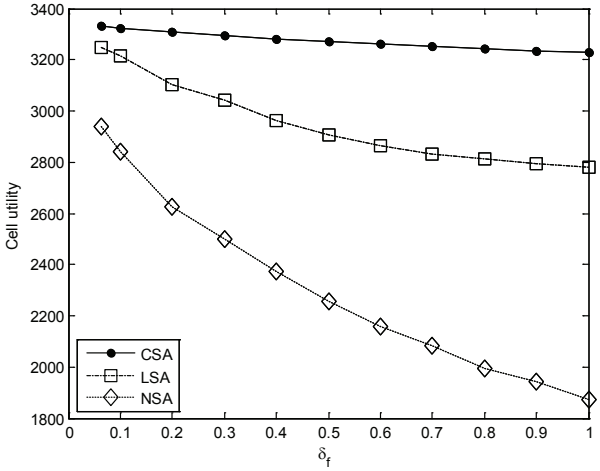

(a) Cell utility

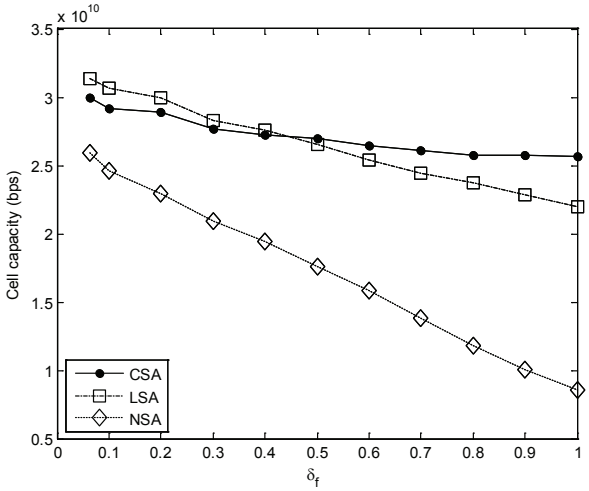

(b) Cell capacity

Figure 7: Performance of CSA, LSA, and NSA, when HeNBs are crowded around MUE. We measure the cell utility and the cell capacity when $N_b = 4$ and $\gamma^{th} = 8$ dB, varying the femtocell density bias δ_f. As δ_f increases, the gap in cell utility between CSA and LSA slightly enlarges, but LSA still significantly outperforms NSA. CSA achieves better cell capacity than LSA with higher δ_f.

Table 2: Definition of Symbols.

Symbol	**Description**
R_m	Macrocell transmission radius
R_f	Femtocell transmission radius
α	Path loss exponent
N_b	Number of beams
g_m	Beamforming gain for the main lobe
g_s	Beamforming gain for the side lobe
ν	Ratio of shared spectrum
$1-\nu$	Ratio of partitioned spectrum
ω_m	utility weights for MUE
ω_f	utility weights for HUE
γ_m	Measured SIR at MUE
γ_f	Measured SIR at HUE
γ_m^{th}	Required SIR at MUE
γ_f^{th}	Required SIR at HUE
d_m^{th}	Macro distance threshold
d_f^{th}	Femto distance threshold
λ_f	Uniform density of femtocells
δ_f	Femtocell density bias
$\mathbf{K_t}$	Set of whole HeNBs
$\mathbf{K_s}$	Set of HeNBs with shared spectrum
$\mathbf{K_p}$	Set of HeNBs with partitioned spectrum
$\mathbf{F_s}$	Set of HeNBs whose distance from MUE is not smaller than d_f^{th}
$\mathbf{M_s}$	Set of HeNBs whose distance from MeNB is not smaller than d_m^{th}